AIAA AVIATION Forum
5-9 June 2017, Denver, Colorado
8th AIAA Theoretical Fluid Mechanics Conference

10.2514/6.2017-4168

Check for updates

Development of adaptive subgrid scale models based on a large-scale vorticity sensor

J.-B. Chapelier[1,*] , C. Scalo[1] and B. Wasistho[2]

[1]*School of Mechanical Engineering and Aeronautical Engineering, Purdue University, IN, USA*

[2]*Kord Technologies, Huntsville, AL, USA*

Downloaded by PURDUE UNIVERSITY on February 2, 2019 | http://arc.aiaa.org | DOI: 10.2514/6.2017-4168

This paper introduces a new approach to Large-Eddy Simulation (LES) where subgrid-scale (SGS) dissipation is applied proportionally to the degree of local spectral broadening, hence mitigated or deactivated in regions dominated by large-scale and/or laminar vortical motion. The proposed coherent-vorticity-preserving (CvP) LES methodology is based on the evaluation of the ratio of the instantaneous test-filtered to resolved (or grid-filtered) enstrophy: $\sigma = \widehat{\overline{\xi}}/\overline{\xi}$. Values of $\sigma \simeq 1$ indicate low sub-test-filter turbulent activity, justifying local deactivation of any subgrid-scale model. Values of $\sigma < 1$ span conditions ranging from incipient spectral broadening $\sigma \lesssim 1$, to equilibrium turbulence $\sigma = \sigma_{eq} < 1$, where σ_{eq} is solely as a function of the test-to-grid filter-width ratio $\widehat{\overline{\Delta}}/\overline{\Delta}$, derived assuming a Kolmogorov's model equilibrium turbulence spectrum. Eddy viscosity is fully restored for $\sigma \leq \sigma_{eq}$. The proposed approach removes unnecessary SGS dissipation, can be applied to any eddy-viscosity model, is algorithmically simple, computationally inexpensive and extendable to non-structured grids. LES of Taylor-Green vortex breakdown demonstrates that the CvP methodology greatly improves the performance of traditional, non-dynamic dissipative SGS models, capturing the peak of total turbulent kinetic energy dissipation during transition. Similar accuracy is obtained by adopting Germano's dynamic procedure albeit at more than twice the computational overhead. Finally, a CvP-LES of a pair of unstable periodic helical vortices, representative of rotor-blade wakes, is considered. The ability of the CvP methodology to dynamically sort the coherent, large-scale motion from the smaller, broadband scales of the flow is demonstrated via flow visualizations.

I. Introduction

In spite of the sustained increase in availability of computational resources, Large-Eddy Simulation (LES) is still the only feasible approach for the numerical investigation of turbulent flows at physically-relevant Reynolds numbers, which are are often out of reach for Direct Numerical Simulations (DNS). The development of accurate and robust sub-grid scale (SGS) models extending the envelope of attainable Reynolds numbers while containing the computational cost is therefore still a warranted effort.

One shortcoming of traditional LES modeling approaches is their tendency to introduce excess SGS dissipation in transitional or locally low-Reynolds-number regions, where the flow is well resolved, or, similarly, impact the evolution of the large coherent vortices which may be on the verge of break-up and transition to turbulence or coexist with finer-scale broadband vorticity. The Smagorinsky model,[1] for example, attenuates velocity gradients at all scales of the flow, resulting in the undesired damping

*Corresponding author, jchapeli@purdue.edu

Copyright © 2017 by J.-B. Chapelier, C. Scalo and B. Wasistho. Published by the American Institute of Aeronautics and Astronautics, Inc. with permission.

Copyright © 2017 by Jean-Baptiste Chapelier, Carlo Scalo and Bono Wasistho. Published by the American Institute of Aeronautics and Astronautics, Inc., with permission.

of coherent laminar vortices or transitional regions. Any accurate SGS model should therefore account only for the energy transfer towards subgrid scales occuring only in the spectral neighborhood of the cutoff wavelength,[2,3] which is challenging for non-spectral-based numerical schemes or even local spatial discretization numerics equipped with dynamic procedures (as discussed later).

A number of approaches aim at correcting the overly dissipative nature of SGS models. The so-called Dynamic procedure and related approaches aim at determining dynamically the subgrid model parameter, leading to an adapation of the subgrid dissipation for transitional or inhomogeneous flows.[4–8] Alternate multiscale approaches aim at applying a low-pass filter on the subgrid tensor in order to reduce the influence of the subgrid dissipation on the large scales of the flow which carry the bulk of kinetic energy. In particular, the high-pass filtered eddy viscosity of Stolz et al.[9] or the VMS approach introduced Hughes et al.[10] have led to important improvement of the subgrid models accuracy. Other authors have proposed to develop sensors attempting to discriminate between laminar and turbulent regions.[11–13] Another approach termed Coherent Vortex Simulation (CVS) uses a wavelet-based decomposition to sort the coherent motion from the Gaussian component of the solution identified as small-scale noise,[14–17] adopting a signal-processing and statistical approach.

Purely numerical approaches have been proposed and rely on the use of regularization procedures such as explicit filtering or addition of artificial viscosity to counter the high-wave-number-energy accumulation occurring in low-dissipation numerical schemes.[18–21]

Other approaches, termed Implicit LES (ILES), aim at tailoring the numerical dissipation naturally present in the adopted numerical discretization, to mimic the sub-grid dissipation deriving from physical SGS models.[22–24] Although resulting in almost no computational overhead, as no explicit execution of subgrid models is needed, such techniques may introduce excessive dissipation,[25,26] with less flexibility than inherently non-dissipative numerical schemes equipped with subgrid models which can be deactivated in dynamically selected regions of the flow. The latter will be the approach followed in this study.

In fact, accurate results at a reduced computational cost have been obtained by coupling high-order finite difference schemes and Dynamic models.[27] Classic Dynamic modeling approaches, however, increase cost, memory requirements and complexity of the implementation, associated with the test-filtering of tensors and averaging of the dynamic parameter along directions of statistical homogeneity[4] or flow path trajectories[6] to obtain stable computations.

We propose in this paper to build a tool detecting the onset of spectral broadening in the flow with a simple and computationally inexpensive turbulence sensor identifying regions of developed, locally high Reynolds number turbulence requiring SGS dissipation. This approach can be seen as a new dynamic approach, blending physics-based SGS modeling with a new scale-selective sensor based on the evaluation of the sub-test-filter enstrophy content. By test-filtering vorticity rather than velocity, a greater sensitivity to the emergence of small-scales in the flow is achieved. By evaluating the ratio of grid- and test-filtered enstrophy, it is possible to quantify the relative small-scale energy content of the flow to then mitigate SGS dissipation in non-turbulent, large-scale narrowband vorticity dominated regions whre coherent or large-scale vortices are likely to be found. The sensor is hence able to discriminate between gradients due to small scale vorticity (most likely broadband turbulence) and large scale structures, which are not governed by inertial subrange transfer energy dynamics assumed by most SGS models. Due to this property we refer to the proposed method as coherent-vorticity-preserving .

The present approach has a number of advantages: (1) the sensor can improve the prediction performance of any existing SGS model in transitional flows; (2) the sensor is based on local and instantaneous flow values, allowing for a dynamic adjustment of the SGS dissipation; (3) the CvP technique is computationally inexpensive, only requiring one addition test-filtering operation on the enstrophy field; (4) algorithmically simple, not requiring any spectral decomposition of the flow and easily extendable to unstructured meshes; (5) allowing for the run-time evaluation of the sub-filter length scale, based on the instantaneous state of turbulence of the flow (not explored in the current study).

The outline of the paper is as follows. First, the LES formalism and numerical methods are detailed in section II. The CvP technique is derived in section III. The various subgrid-scale models used in

Downloaded by PURDUE UNIVERSITY on February 2, 2019 | http://arc.aiaa.org | DOI: 10.2514/6.2017-4168

the study are reported in section III.B. Section IV features a study of the CvP technique considering LES of transitional Taylor-Green vortex. The sensor is coupled to various traditional dissipative SGS models, and compared to the classical Dynamic model. The approach is then applied to a periodic double helical vortex configuration (section V), which is a model problem for rotor blade vortices. The ability of the sensor function to sort the coherent structures from the broadband, small-scale turbulence is also assessed with instantaneous visualizations.

II. Numerics

A. Filtered Navier-Stokes equations

In this work, the compressible fluid motion is simulated by discretizing the Navier-Stokes operator $\mathcal{NS}(\mathbf{w})$, which can be cast in the form:

$$\mathcal{NS}(\mathbf{w}) = \frac{\partial \mathbf{w}}{\partial t} + \boldsymbol{\nabla} \cdot [\mathbf{F}_{\mathrm{c}}(\mathbf{w}) - \mathbf{F}_{\mathrm{v}}(\mathbf{w}, \nabla \mathbf{w})] = \mathbf{0}, \tag{1}$$

where $\mathbf{w} = (\rho, \rho\mathbf{U}, \rho E)^{\mathrm{T}}$ is the vector of conserved variables ρ, $\mathbf{U}$ and E, density, velocity and total energy respectively, and $(\nabla \mathbf{w})_{ij} = \partial w_i / \partial x_j$ its gradient. The viscous and convective flux tensors $\mathbf{F}_{\mathrm{c}}, \mathbf{F}_{\mathrm{v}} \in \mathbb{R}^{5\times 3}$ read

$$\mathbf{F}_{\mathrm{c}} = \begin{pmatrix} \rho\mathbf{U}^{\mathrm{T}} \\ \rho\mathbf{U} \otimes \mathbf{U} + p\mathbf{I} \\ (\rho E + p)\mathbf{U}^{\mathrm{T}} \end{pmatrix}, \quad \text{and} \quad \mathbf{F}_{\mathrm{v}} = \begin{pmatrix} \mathbf{0} \\ \boldsymbol{\tau} \\ \boldsymbol{\tau} \cdot \mathbf{U} - \lambda \boldsymbol{\nabla} T^{\mathrm{T}} \end{pmatrix}, \tag{2}$$

where T is the temperature, p is the pressure, λ is the thermal conductivity of the fluid and $\mathbf{I} \in \mathbb{R}^{3\times 3}$ is the identity matrix. For a Newtonian fluid, we have

$$\boldsymbol{\tau} = 2\mu \mathbf{S}, \tag{3}$$

where μ is the dynamic viscosity and

$$\mathbf{S} = \frac{1}{2}\left[\nabla \mathbf{U} + \nabla \mathbf{U}^{\mathrm{T}} - \frac{2}{3}(\boldsymbol{\nabla} \cdot \mathbf{U})\mathbf{I}\right]. \tag{4}$$

The ideal gas law is considered for the closure of the system of equations, namely,

$$p = (\gamma - 1)\left(\rho E - \frac{1}{2}\rho \mathbf{U} \cdot \mathbf{U}\right), \tag{5}$$

where γ is the heat capacity ratio.

The LES equations are obtained by applying a low-pass filter to the Navier-Stokes equations.[28] The spatial filtering operator applied to a generic quantity ϕ reads

$$\overline{\phi}(\mathbf{x}, t) = g(\mathbf{x}) \star \phi(\mathbf{x}), \tag{6}$$

where $\star$ is the convolution product and $g(\mathbf{x})$ is a filter kernel related to a cutoff length scale $\overline{\Delta}$ in physical space.[3] The compressible case requires density-weighted filtering approaches. The density-weighted or Favre filtering operator is defined as

$$\widetilde{\phi} = \frac{\overline{\rho\phi}}{\overline{\rho}}. \tag{7}$$

In the present study, the compressible LES formalism introduced by Lesieur et al.[29–31] is adopted yielding the following set of filtered compressible Navier-Stokes equations:

$$\mathcal{NS}(\overline{\mathbf{w}}) = \boldsymbol{\nabla} \cdot \mathbf{F}_{\mathrm{SGS}}(\overline{\mathbf{w}}, \nabla \overline{\mathbf{w}}), \tag{8}$$

Downloaded by PURDUE UNIVERSITY on February 2, 2019 | http://arc.aiaa.org | DOI: 10.2514/6.2017-4168

Filter	$\widehat{\overline{\Delta}}$	α	a	b	c	d	e
IMPL6	$1.5\overline{\Delta}$	α	$\frac{1}{16}(11+10\alpha)$	$\frac{1}{32}(15+34\alpha)$	$\frac{1}{16}(-3+6\alpha)$	$\frac{1}{32}(1-2\alpha)$	0

Table 1. Finite difference coefficients for the LES test filter.

where $\overline{\mathbf{w}} = \left(\overline{\rho}, \overline{\rho}\widetilde{\mathbf{U}}, \overline{\rho}\widetilde{E}\right)^{\mathrm{T}}$ is the vector of filtered conservative variables.

The SGS tensor $\mathbf{F}_{\mathrm{SGS}}$ is the result of the filtering operation and it encapsulates the dynamics of the unresolved sub-grid scales, and is modeled here using the eddy-viscosity assumption:

$$\mathbf{F}_{\mathrm{SGS}}(\overline{\mathbf{w}}, \nabla\overline{\mathbf{w}}) = \begin{pmatrix} \mathbf{0} \\ 2\mu_t\overline{\mathbf{S}} \\ -\frac{\mu_t C_p}{Pr_t}\boldsymbol{\nabla}\widetilde{T}^{\mathrm{T}} \end{pmatrix}, \tag{9}$$

where $\overline{\mathbf{S}}$ is the shear stress tensor computed from equation (4) based on the Favre-filtered velocity $\widetilde{\mathbf{U}}$, Pr_t is the turbulent Prandtl number, which is set to 0.5,[32] C_p is the heat capacity at constant pressure of the fluid and μ_t is the eddy-viscosity which depends on the chosen sub-grid model.

The only assumption required to derive (8) is that the filtering operation (6) commutes with spatial derivatives. The various filtering and discretization strategies adopted in the current work are outlined in the following sections.

B. Numerical Discretization

The compressible, Favre-filtered Navier-Stokes equations are solved using a 6th order compact finite difference scheme solver originally written by Nagarajan *et al.*,[27] currently under development at Purdue University. The solver is based on the staggered grid arrangement, providing superior accuracy compared to a fully collocated approach.[33]

The time integration is performed using a third order Runge-Kutta scheme.

C. Filtering Strategy

The new LES model presented in this paper requires the implementation of a test-filter to sort the large-scale motion from the small-scale, broadband turbulence. The generic formulation for the computation of the test-filtered quantities read:

$$\alpha f_{i-1}^{\mathrm{TF}} + f_i^{\mathrm{TF}} + \alpha f_{i+1}^{\mathrm{TF}} = af_i + \frac{b}{2}(f_{i+1}+f_{i-1}) + \frac{c}{2}(f_{i+2}+f_{i-2}) + \frac{d}{2}(f_{i+3}+f_{i-3}) + \frac{e}{2}(f_{i+3}+f_{i-3}), \tag{10}$$

In the present study, the test filter considered is a sixth-order, spatially implicit compact filter introduced by Lele,[33] which coefficients are detailed in Table 1. This filter is characterized by non-zero values of the parameter $\alpha \in]-0.5, 0.5[$, which controls the strength of the test filter. Weaker filters are obtained using high values of α and vice-versa. For the present study, the parameter α is set to -0.4 which yields a large-scale selective test filtering. This filter is named IMPL6 for the rest of the paper. Its filter length is $\widehat{\overline{\Delta}}_{\mathrm{IMPL6}} = 1.5\Delta$, as defined by the cutoff wavenumber verifying $G(\widehat{\overline{k}}\Delta) = 0.5$, where $\widehat{\overline{k}} = \pi/\ \widehat{\overline{\Delta}}$.

Downloaded by PURDUE UNIVERSITY on February 2, 2019 | http://arc.aiaa.org | DOI: 10.2514/6.2017-4168

Downloaded by PURDUE UNIVERSITY on February 2, 2019 | http://arc.aiaa.org | DOI: 10.2514/6.2017-4168

III. Coherent-vorticity-preserving (CvP) Eddy Viscosity Correction

A. CvP Model derivation

In this section, a new idea for the developement of a turbulence sensor able to discriminate between coherent and broadband turbulence is presented. This sensor is based on the detection of vorticity in the range of scales located between the primary and test filter cutoff lengths. The primary filtering is assumed to be performed by the computational grid and its cutoff length is $\overline{\Delta} = \Delta$, which is the cell size. The test-filter is defined in order to isolate large scales and its cutoff length $\widehat{\overline{\Delta}}$ is therefore greater than $\overline{\Delta}$.

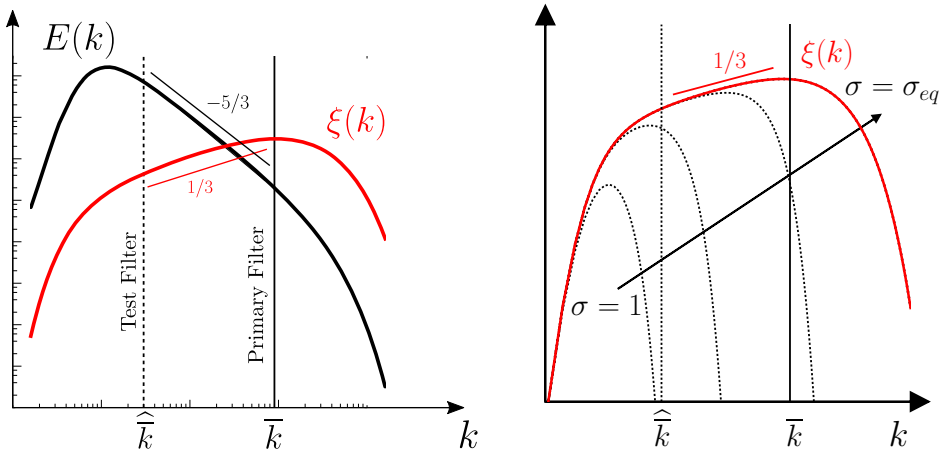

Figure 1. Schematic view of energy and enstrophy spectra for high Reynolds, isotropic turbulence.

In an idealized incompressible, fully developed isotropic turbulent flow, the energy cascade leads to a transfer of energy from the large scales towards the small scales of the flow, which is associated to a broadband energy spectrum scaling as $k^{-5/3}$ in the inertial range. This particular distribution of the energy in the spectral space implies that most of the energetic content of the flow is carried by the large scales. At the contrary, the spectral content of enstrophy grows as $k^{1/3}$, showing a peak at the small-scale level. In developed turbulent flows, the enstrophy levels are therefore mostly governed by the small-scale activity of the flow.

For a general derivation of the sensor, the present analysis is focused on the enstrophy $\xi = \boldsymbol{\omega} \cdot \boldsymbol{\omega}/2$. The sensor is built following simple observations:

- If $\hat{\bar{\xi}} \approx \bar{\xi}$, no vorticity is detected at the small-scale level, yielding a local deactivation of the subgrid model.
- At the contrary, if $\hat{\bar{\xi}} \ll \bar{\xi}$, an intense small-scale vortical activity is detected, enabling local application of the subgrid dissipation.

The next step consists in creating a function f of the ratio $\sigma = \hat{\bar{\xi}}/\bar{\xi}$ which will act as a turbulence sensor. Based on the first observation, a lower bound for f can be defined as $f(\sigma = 1) = 0$ when the test filtered enstrophy is equal to the explicitly filtered enstrophy. The upper bound of f can be calibrated by finding a value for σ assuming a situation of fully developed isotropic turbulence. In this case, the expression of filtered enstrophy for isotropic turbulence reads:

$$\bar{\xi} = \int_0^\infty k^2 E(k) \bar{G}^2(k) dk \tag{11}$$

Substituting the expression of the Kolmogorov spectrum, the value for σ corresponding to an equilibrium energy cascade becomes:

$$\sigma_{eq} = \frac{\int_0^\infty (k\Delta)^{1/3} \hat{G}(k\Delta) \bar{G}^2(k\Delta) dk\Delta}{\int_0^\infty (k\Delta)^{1/3} \bar{G}^2(k\Delta) dk\Delta} \tag{12}$$

The upper bound for the sensor becomes $f(\sigma = \sigma_{eq}) = 1$. The following shape for f is proposed:

$$f(\sigma) = \begin{cases} 1 & \text{for} \quad \sigma < \sigma_{eq}, \\ \frac{1}{2}\left(1 + \sin\left(\pi \frac{\sigma_{eq} - 2\sigma + 1}{2(1-\sigma_{eq})}\right)\right) & \text{for} \quad \sigma \in [\sigma_{eq}, 1], \\ 0 & \text{for} \quad \sigma > 1. \end{cases} \tag{13}$$

This shape guarantees a smooth scale-separation between large scale vortices and small-scale turbulence. It can be seen as multiple filtering levels embedded in one single function that shows low values in regions dominated by large-scales and progressively higher values as the small scales develop corresponding to higher wavenumbers.

An adaptation of the subgrid model intensity can therefore be achieved by multiplying the eddy viscosity by the sensor function:

$$\mu_t^\star = f \mu_t \tag{14}$$

This particular expression will lead to a decrease of the eddy viscosity in transitional and smooth regions of the flow and a progressive increase depending on the extent of the small-scale dynamics at a given location.

We first derive the general expression of σ_{eq} assuming that the grid and test filters are sharp in spectral space with respective filter lengths of $\overline{\Delta}$ and $\widehat{\overline{\Delta}}$. The ratio of the two filter lengths is defined as $r_\Delta = \widehat{\overline{\Delta}}/\overline{\Delta}$. This yields the following expression for σ_{eq}:

$$\sigma_{eq} = \frac{\int_0^{\pi/r_\Delta} (k\Delta)^{1/3} dk\Delta}{\int_0^{\pi} (k\Delta)^{1/3} dk\Delta} = r_\Delta^{-4/3} \tag{15}$$

This result is consistent with the fact that a smaller bandwith for test-filtered scales (high values of r_Δ) lead to an activation of the sensor for a broader range of small-scales.

In the present paper, an additional tuning of the model calibration adapted to the present numerical is performed, by considering the analytical expression of the test filter transfer function and the interpolation operator. The numerical method employed requires the interpolation of the vorticity components on the density locations in order to compute the values of enstrophy. This sixth order compact interpolation operator is described in Nagarajan *et al.*[27] This operator introduces a damping of a part of the small-scale content of enstrophy, which can be taken into account in the calibration of the model:

$$\sigma_{eq} = \frac{\int_0^\infty (k\Delta)^{1/3} \hat{G}(k\Delta) G^{\text{int}}(k\Delta) dk\Delta}{\int_0^\infty (k\Delta)^{1/3} G^{\text{int}}(k\Delta) dk\Delta} \tag{16}$$

where G^{int} is the transfer function from the interpolant. The analytical expression of the test filter transfer function defined in Section II.C is substituted in 16 to find the corresponding values of σ_{eq}. This value is 0.71 for the IMPL6 test fiter.

B. Subgrid scale models

This section presents the various dissipative SGS models based on the eddy viscosity assumption that are enhanced using the CvP methodology.

Downloaded by PURDUE UNIVERSITY on February 2, 2019 | http://arc.aiaa.org | DOI: 10.2514/6.2017-4168

Downloaded by PURDUE UNIVERSITY on February 2, 2019 | http://arc.aiaa.org | DOI: 10.2514/6.2017-4168

1. Smagorinsky

The most commonly employed dissipative SGS model is the Smagorinsky model for which the eddy viscosity reads:

$$\mu_t = \rho(\mathrm{C_S}\Delta)^2\sqrt{\bar{\mathbf{S}}:\bar{\mathbf{S}}} \tag{17}$$

where $\mathrm{C_S}$ is the Smagorinsky parameter, Δ the filter width. $\mathrm{C_S}$ is usually calibrated assuming an isotropic turbulence field associated with the infinite Reynolds-number, equilibrum Komogorov spectrum. In this particular case, and assuming that the discretization is equivalent to a sharp filtering of width Δ, the value of the Smagorinsky parameter is $C_S = 0.172$.

2. Structure function

The second model considered is the structure function model introduced by Metais and Lesieur.[34] For this particular model, the eddy viscosity is built from the evaluation of the second order structure function of the velocity vector:

$$\mu_t = 0.105{\mathrm{C_K}}^{-3/2}\sqrt{\bar{F}_2(\Delta)} \tag{18}$$

where $\mathrm{C_K}$ is the Kolmogorov constant (here set to 1.5) and $\bar{F}_2(\Delta) = \left\langle||\bar{\mathbf{u}}(\mathbf{x}) - \bar{\mathbf{u}}(\mathbf{x}+\mathbf{r}))||^2\right\rangle_{||\mathbf{r}||=\Delta}$. $< \cdot >$ is an averaging operator involving the values on the six points surrounding the actual point where the structure function is computed. This model is expected to be less dissipative than the Smagorinsky model in transitional regions and more dissipative in vortex cores.

3. Vreman

The last model considered for the evaluation of the turbulence sensor is the model introduced by Vreman.[35] This model displays interesting features such as the vanishing of the subgrid dissipation in pure shear regions and correct near wall turbulence scaling. The eddy viscosity reads:

$$\mu_t = \rho(2.5\mathrm{C_S}\Delta)^2\sqrt{\frac{B_\beta}{\alpha_{ij}\alpha_{ij}}} \tag{19}$$

where $\alpha_{ij} = \partial_j u_i$ is the velocity gradient tensor, $\beta_{ij} = \alpha_{mi}\alpha_{mj}$ and $B_\beta = \beta_{11}\beta_{22} - \beta_{12}^2 + \beta_{11}\beta_{33} - \beta_{13}^2 + \beta_{22}\beta_{33} - \beta_{23}^2$.

4. Dynamic model

In order to provide a comparison of the present approach with a well known, comparable approach, the Dynamic Smagorinsky version of Spyropoulos and Blaisdell[36] is implemented. For this model, the eddy viscosity reads:

$$\mu_t = \rho\mathrm{C_D}\sqrt{\bar{\mathbf{S}}:\bar{\mathbf{S}}} \tag{20}$$

where $\mathrm{C_D}$ is the dynamic parameter, defined as follows:[37]

$$\mathrm{C_D} = \frac{\langle L_{ij}M_{ij}\rangle}{\langle M_{kl}M_{kl}\rangle} \tag{21}$$

where $< \cdot >$ is a spatial averaging operator acting over directions of statistical homogeneity and L_{ij}, M_{ij} are operators defined as in Spyropoulos and Blaisdell.[36] The test filter used to computed M_{ij} and L_{ij} is the IMPL6 compact filter described in section II.C .

Downloaded by PURDUE UNIVERSITY on February 2, 2019 | http://arc.aiaa.org | DOI: 10.2514/6.2017-4168

IV. LES of Taylor-Green vortex breakdown

A. Problem definition

The Taylor-Green vortex flow features the transition of initially large-scale vortices which progressively breakdown into small-scale turbulence. This configuration is therefore of interest to assess the ability of subgrid models to both characterize accurately transition and fully developed turbulencd. The initial conditions are analytically defined in a cubic domain $(2\pi L)^3$ and read:

$$\mathbf{U}(\mathbf{x},0) = \begin{pmatrix} V_0 \sin(x/L)\cos(y/L)\cos(z/L) \\ -V_0 \cos(x/L)\sin(y/L)\cos(z/L) \\ 0 \end{pmatrix}, \tag{22}$$

$$\mathrm{p}(\mathbf{x},0) = \mathrm{p}_0 + \frac{\rho_0 V_0^2}{16}\left[\cos(2x/L)+\cos(2y/L)\right]\left(\cos(2z/L)+2\right). \tag{23}$$

$$\rho(\mathbf{x},0) = \rho_0. \tag{24}$$

All the relevant quantities are normalized by the reference length L, velocity magnitude V_0 and density ρ_0. The Reynolds number $Re = \rho_0 V_0 L/\mu_0$ is case-specific and the Mach number $M = V_0/\sqrt{\gamma\, P_0/\rho_0}$ is fixed to the value 0.1, leading to mostly incompressible dynamics. The state of turbulence is monitored by evaluating the temporal evolution of the volume-averaged total kinetic energy E and the dissipation rate ε:

$$E(t) = \frac{1}{2\mathrm{V}}\int_{\mathrm{V}} \mathbf{u}(\mathbf{x},t)\cdot\mathbf{u}(\mathbf{x},t)d\mathbf{x} \tag{25}$$

$$\varepsilon(t) = \frac{dE(t)}{dt} \tag{26}$$

The temporal evolution of spatially integrated subgrid dissipation $\varepsilon_{\mathrm{SGS}}$ is considered as well to determine the intensity of the modeled subgrid scales introduced by each LES models.

$$\varepsilon_{\mathrm{SGS}}(\mathbf{x},t) = \frac{1}{\mathrm{V}}\int_{\mathrm{V}} \mu_t \mathbf{S}:\mathbf{S}d\mathbf{x} \tag{27}$$

B. Evaluation of the sensor accuracy

In this section, the accuracy of the CvP approach coupled with the Smagorinsky model is evaluated in comparison with the Dynamic model. The Reynolds number is set to 5000 and the DNS performed by Chapelier and Lodato[13] featuring 480^3 degrees of freedom is chosen as the reference computation. The LES discretization features 72^3 grid points and computations are performed with the baseline Smagorinsky model, the new model coupling the turbulence sensor and Smagorinsky, the Dynamic model and without SGS model (termed no model computation). It is notable that the resolution is more than six times coarser in each direction for the LES discretization when compared to the reference DNS.

Figure 2 depicts the evolution of mean turbulent kinetic energy (or TKE) and dissipation for the three LES computations and the DNS. The DNS energy is filtered using a spectral sharp cutoff filter corresponding to the LES grid size. The DNS filtered dissipation is obtained by the means of the temporal derivative of the filtered DNS energy. The no-model computation lacks dissipation which leads to a blow-up of the TKE and negative values of dissipation. The Smagorinsky, at the contrary, introduces an excessive amount of subgrid dissipation which impacts the development of the small-scale vortices in the flow, as seen on the evolution of the dissipation. The Smagorinsky model based on the new sensor developed successfully improves the baseline model and provides an accurate prediction of the evolution of both quantities. Figure 3 presents the temporal evolution of the mean values of the subgrid dissipation and f. The subgrid dissipation for the sensor and dynamic models is efficiently lowered at the beginning of the computation as opposed to the Smagorinsky computation

which introduces significant amounts of dissipation affecting the dynamics of the flow. It is found that $f(\sigma)$ is low at the beginning of the computation, showing that the sensor successfully detects the presence of large coherent vortices and mitigates the subgrid dissipation accordingly.

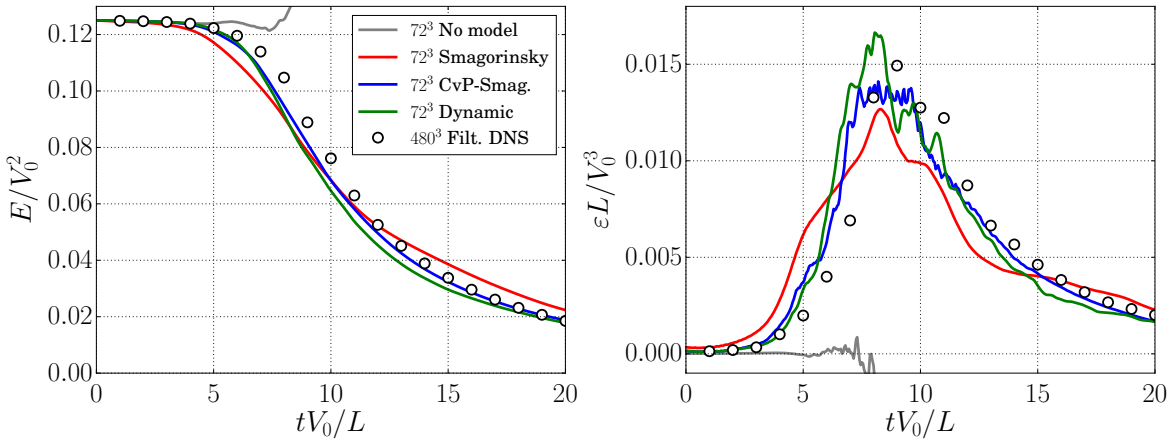

Figure 2. Evolution of the turbulent kinetic energy and dissipation for the LES of the Taylor-Green vortex.

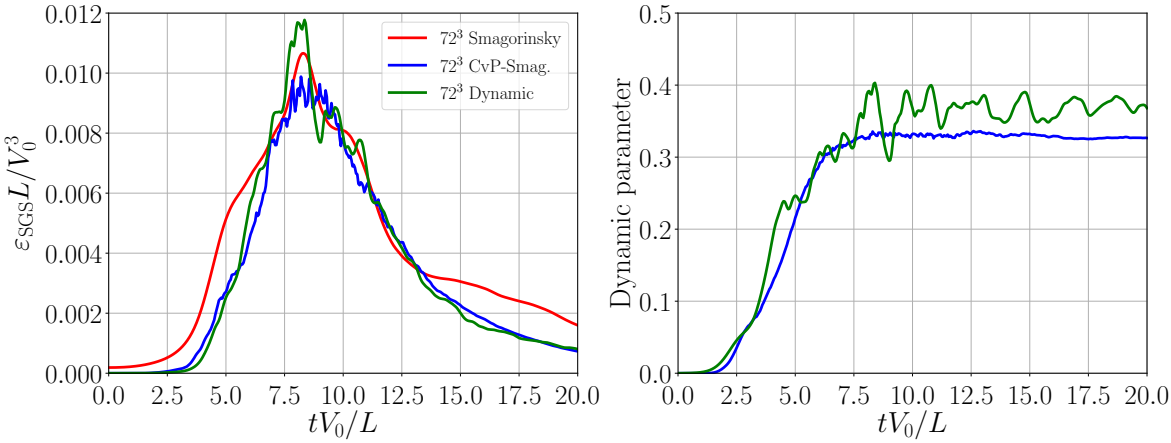

Figure 3. Temporal evolution of the subgrid dissipation (left) and the mean dynamic parameter defined as the factor of the classical Smagorinsky eddy viscosity ($\langle f \rangle$ for the sensor and $C_D/(C_S\Delta)^2$ for the Dynamic model)(right) for the LES of the Taylor-Green vortex flow.

The energy spectra between $tV_0/L = 8$ and $tV_0/L = 20$ are plotted in Figure 4. At $t = 8$, near the peak of enstrophy, while all models provide an good approximation of the large-scale dynamics, the small-scale energy is significantly damped for the Smagorinsky computation. The Dynamic and CvP computations improve greatly the behavior of the Smagorinsky model and show a good match with the DNS at the small-scale level. The CvP-LES approach is slightly more accurate than the Dynamic model in the midrange of the energy spectrum. The two models also exhibit a slight high-wavenumber pile-up of energy, more pronounced for the Dynamic model. This phenomenon due to aliasing errors is probably the cause of the excess of mean enstrophy found for the Dynamic model computation. At later times, the Smagorinsky model shows an imbalance of spectral energy distribution, with a corresponding overestimation and damping of the large and small-scale energy respectively. The strong damping of small-scale energy is likely to create a bottleneck effect that blocks the energy transfers, causing such

Downloaded by PURDUE UNIVERSITY on February 2, 2019 | http://arc.aiaa.org | DOI: 10.2514/6.2017-4168

a spectral energy imbalance. The energy spectra at late times are more accurate for the Dynamic and CvP models, and the CvP in particular leads to an excellent representation of the large-scale energy for long time integration (especially seen at $t = 16$).

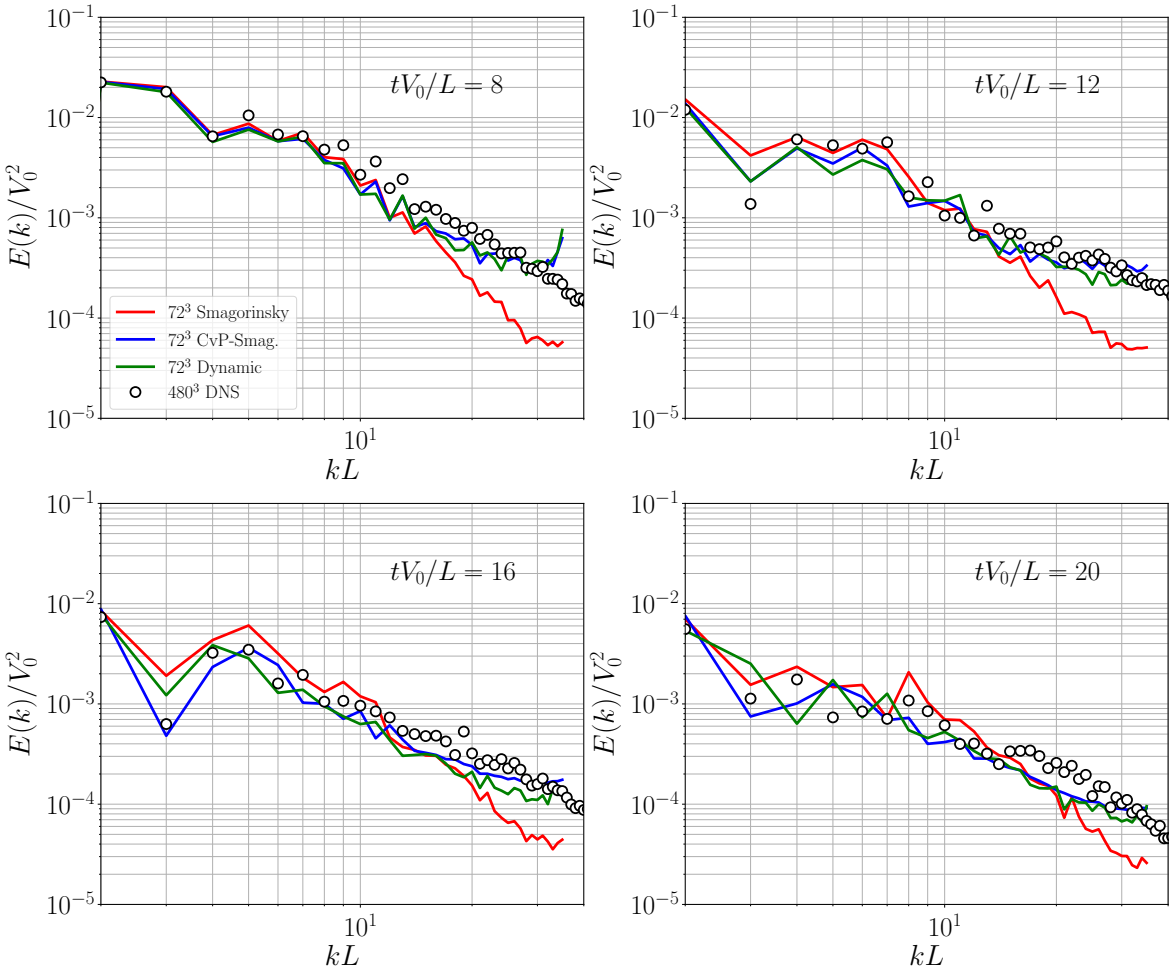

Figure 4. Energy spectra at various times for the LES of the Taylor-Green vortex at $Re = 5000$. Subgrid models comparison using a 72^3 grid.

C. Subgrid models efficiency

In this section, the costs of the different subgrid modeling approaches adressed in the previous section are assessed in terms of CPU time. The calculations on the 72^3 where performed on parallel architectures using 16 computational cores. For the determination of the models efficiency, sample computations are run without any code output which could slow down artificially the performance of the runs. The no-model CPU time is chosen as the reference as it is the faster run. Table 2 report the relative CPU times for the no-model, Smagorinsky , sensor and Dynamic models runs. As expected, a CPU time overhead is observed when SGS models are used compared to the no-model computation. What is remarkable is that the sensor computation CPU overhead is extremely close to the one observed for the baseline Smagorinsky. This shows that the computation of the sensor function is inexpensive, which was expected as the only costly step is the test filtering of the enstrophy. The Dynamic model is found to be much more CPU intensive, leading to a computational time overhead

Downloaded by PURDUE UNIVERSITY on February 2, 2019 | http://arc.aiaa.org | DOI: 10.2514/6.2017-4168

Model	CPU Time	Computational overhead
No subgrid model	t_{ref}	-
Smagorinsky	$1.134t_{ref}$	+13.4%
Smagorinsky + sensor	$1.151t_{ref}$	+15.1%
Dynamic model	$1.404t_{ref}$	+40.4%

Table 2. Computational time for the various modeling approaches considered for the Taylor-Green vortex computations using a 72^3 grid.

of 40 percent compared to the no-model computation. This excessive cost is due to need of test filtering each occurence of the tensor M_{ij} and averaging globally the numerator and denominator of the dynamic coefficient expression.

D. Influence of the subgrid model

In the present section, the ability of the CvP methodology to enhance the performance of various subgrid models is assessed. The Smagorinsky model, Structure Function and Vreman (all described in section III.B) models are considered. Fig. 5 presents the evolution of mean enstrophy and subgrid dissipation for the baseline and sensor computations. The baseline Smagorinsky and Structure function models lead to similar results, which is expected for freely decaying turbulence. Both models introduce a strong subgrid dissipation which lead to an erroneous prediction of dissipation at the early stages of the computations, emphasizing their inaptitude to capture the transient features of the flow (characterized by a model subgrid dissipation active during the transition). The Vreman model leads to a slightly more accurate prediction of the evolution of the dissipation rate. It appears that for all models considered, the CvP sensor yields a clear improvement in the prediction of the dissipation rate. In particular, Figure 6 shows the evolution of the sensor function values and the improved models are found to successfully reduce the subgrid dissipation at the early stages, leading to a much more accurate prediction of the transition to fully developed turbulence.

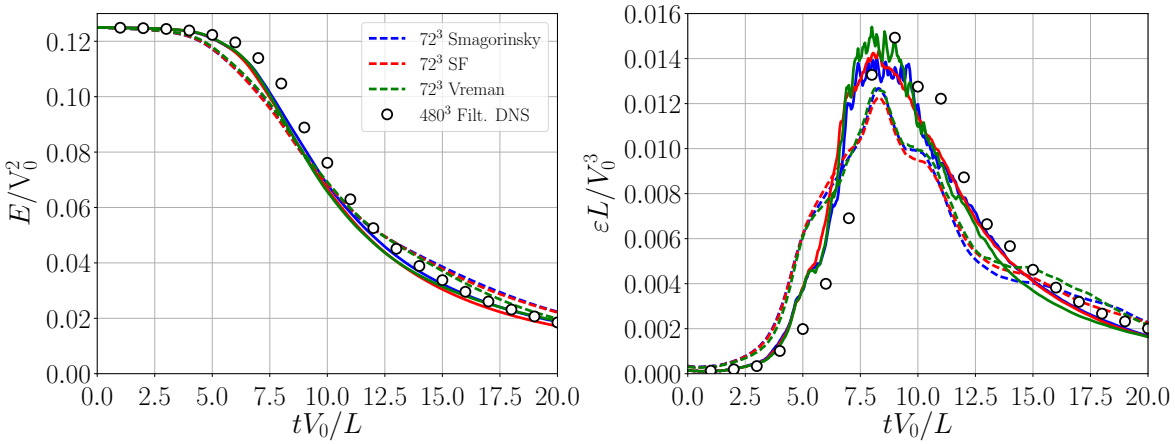

Figure 5. Mean kinetic energy (left) and dissipation (right) for CvP (solid lines) and non-CvP (dashed lines) LES computations of the Taylor-Green vortex at $Re = 5000$.

Downloaded by PURDUE UNIVERSITY on February 2, 2019 | http://arc.aiaa.org | DOI: 10.2514/6.2017-4168

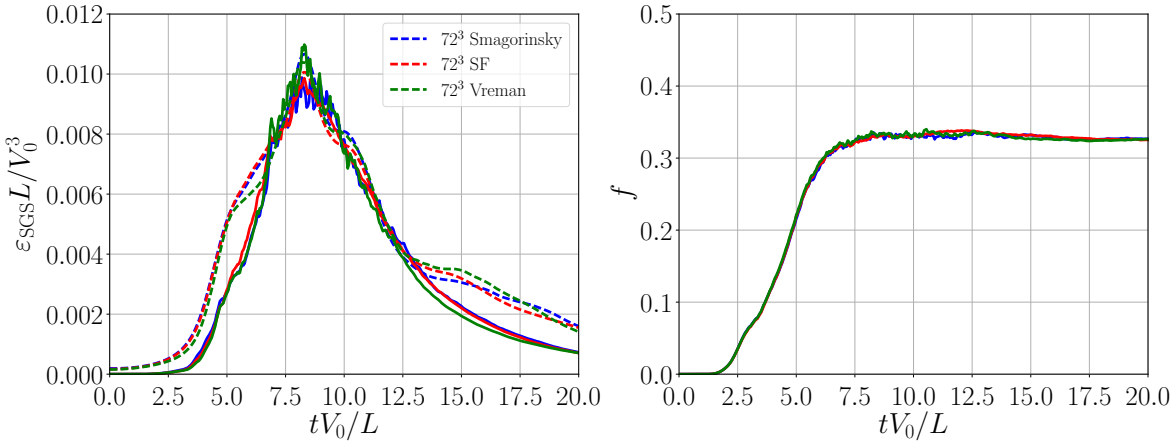

Figure 6. Temporal evolution of the subgrid dissipation (left) and dynamic parameter (right) defined as the factor of the classical Smagorinsky eddy viscosity ($\langle f \rangle$ for the sensor and $C_D/(C_S\Delta)^2$ for the Dynamic model) for the LES of the Taylor-Green vortex flow.

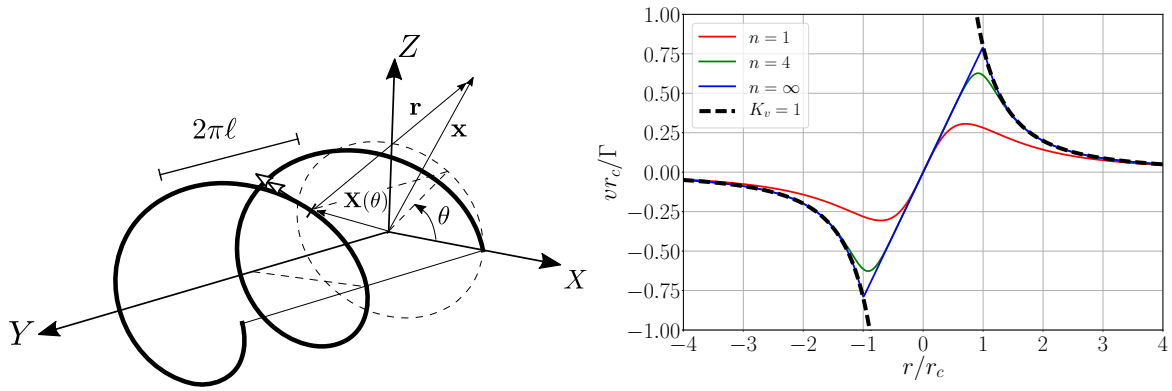

Figure 7. Helical vortex setup (left), radial velocity profile for the Biot-Savart law with modified Kernel function to account for the viscous core (right).

V. LES of Double helical vortex breakdown

A. Problem definition

In this section, a fundamental test case is defined for the study of helices that are representative of vortices generated in the wake of rotating devices. A vortex filament is initialized in a periodic, cubic box. The filament equation reads:

$$\mathbf{X}(\theta) = [\ell\theta, R\cos(\theta), R\sin(\theta)] \tag{28}$$

where R is the radius and h is the pitch of the helix. The velocity field induced by the vortex filament is determined by the Biot-Savart law.

$$\mathbf{u}(\mathbf{x}) = -\frac{\Gamma}{4\pi}\int K_v \frac{(\mathbf{x}-\mathbf{X}(\theta))\times\mathbf{t}(\theta)}{|\mathbf{x}-\mathbf{X}(\theta)|^3}d\theta \tag{29}$$

Downloaded by PURDUE UNIVERSITY on February 2, 2019 | http://arc.aiaa.org | DOI: 10.2514/6.2017-4168

where $\mathbf{t}(\theta) = (-R\sin\theta, R\cos\theta, \ell)$ is the tangent vector to the helical filament, Γ is the circulation and K_v is a function allowing to define the shape of the vortex core[38] and reads:

$$K_v = \frac{|\mathbf{x} - \mathbf{X}(\theta)|^3}{\left(|\mathbf{x} - \mathbf{X}(\theta)|^{2n} + r_c^{2n}\right)^{\frac{3}{2n}}} \tag{30}$$

where σ is the core radius. The case $n = \infty$ corresponds to a Rankine vortex. The value of $n = 4$ is adopted to achieve a smooth transition between the inner, rotational flow and the outer, potential flow. The corresponding plots of transverse velocity v as a function of the radius are shown in Figure 7 for different values of n and for the case $K_v = 1$ which corresponds to the Biot-Savart law without correction, leading to infinite velocity at the core of the vortex.

B. Validation against experiments

In this section, the experimental conditions of the double helical vortex studied by Nemes et al.[39] are tentatively reproduced using the presently developed numerical framework. The radius of the helix is $R = 0.115$, as in the experiment. The ratio of the helical pitch to helix radius is set to $h/R = 1.1$ which guarantees an unstable configuration due to the mutual inductance phenomenon. The ratio of the vortex core radius to helix radius is set to $r_c/R = 0.06$ to match the experimental conditions. Finally, the circulation is defined by the means of the Reynolds number based on the circulation $Re_\Gamma = \Gamma/\nu = 7000$. The direct numerical simulation of this flow being intractable due to the Reynolds considered, a LES is performed using the sensor approach coupled to the Smagorinsky model using a 128^3 grid and a cubic box of dimensions 0.5^3. This leads to the definition of about 3 grid points inside the vortex cores. First, the capacity of the sensor function to identify the large scale motion of the flow is assessed by plotting vorticity iso-surfaces colored by the sensor function. Figure 8 presents the iso-surfaces at four different times. At the beginning of the computation, only large scale features dominated the flow. The onset of small-scales due to the instability caused by mutual inductance is visible at the time $t = 6$. For the early stages of the computation, the iso-surfaces are mainly colored in black, meaning that the sensor function is mostly inactive. When the flow transitions and small-scales develop, high-vales of the sensor function characterized by white regions start to appear. What is remarkable is the ability of the sensor function to separate the small-scales, mainly colored in white, from the coherent motion characterized by a black color. This feature is also visible at $t = 8$, when the large scales begin to vanish and the small-scale motion becomes prominent. It is also observed that although the coherent vortices are mainly colored in black, they show white spots that are related with an activation of the subgrid dissipation on these vortices. This is possibly due to the sharp variations of the sensor function, and future work could adress this problem, by for example filtering or smoothing the function. Furthers vizualisations in Figures 9,10 show the iso-surface of vorticity clipped, corresponding respectively to low and high values of the sensor function. These plots confirm that the sensor function is successful at identifying correctly the coherent motion of the flow. First, the tracking of coherent motion through time is well identified by low values of f as seen on the left column of Figures 9,10. Then, it is also particularly seen from the right column plots of Figures 9,10 that high-values of f monitor the progressive onset of small-scales as time evolves and as coherent vortices breakdown to fully developed turbulence.

Downloaded by PURDUE UNIVERSITY on February 2, 2019 | http://arc.aiaa.org | DOI: 10.2514/6.2017-4168

Downloaded by PURDUE UNIVERSITY on February 2, 2019 | http://arc.aiaa.org | DOI: 10.2514/6.2017-4168

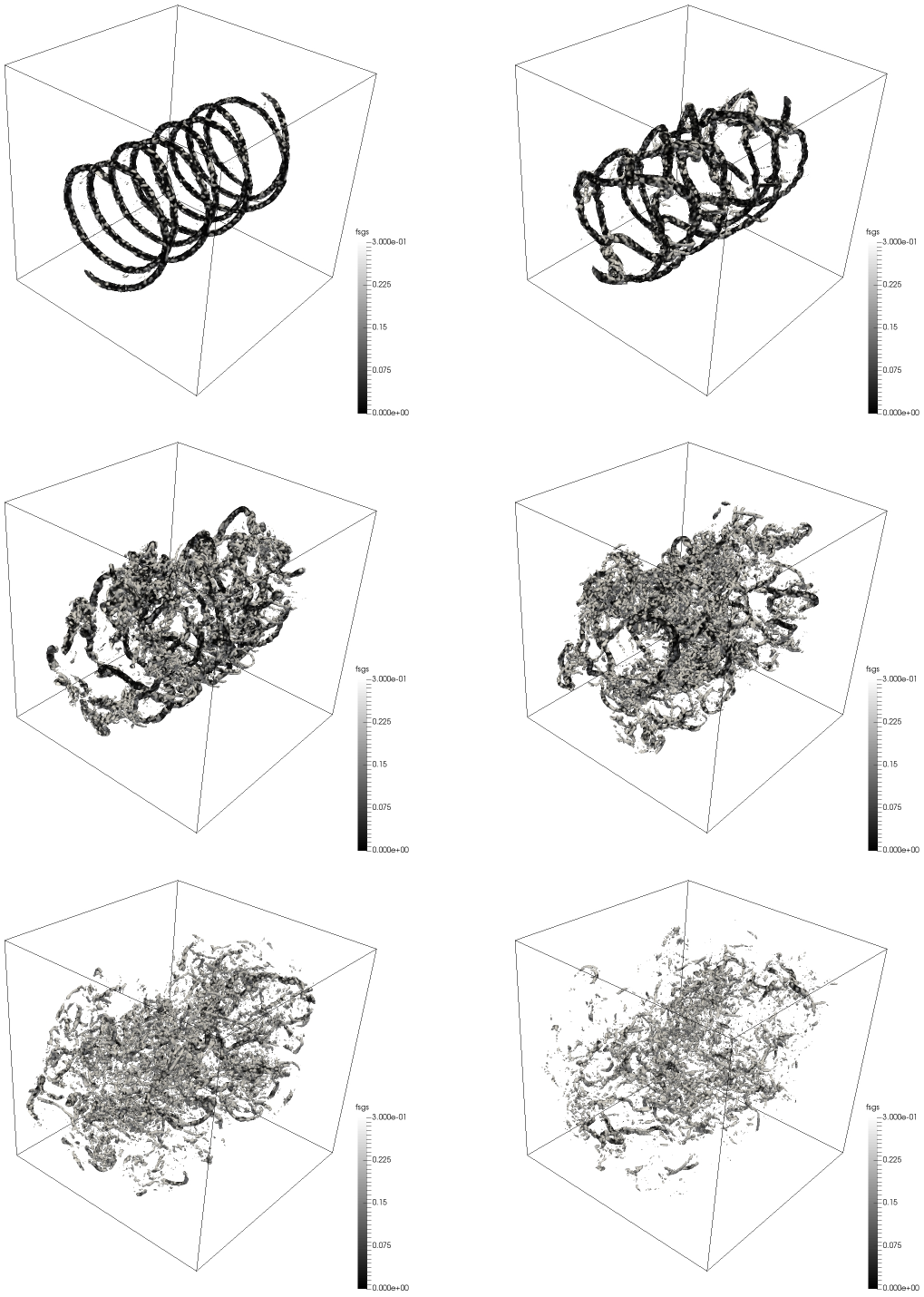

Figure 8. Iso-surfaces of vorticity colored by the sensor function at different times for the LES of the double helix configuration. From top to bottom and left to right: $t = 2, 4, 6, 8, 10, 12$**.**

Downloaded by PURDUE UNIVERSITY on February 2, 2019 | http://arc.aiaa.org | DOI: 10.2514/6.2017-4168

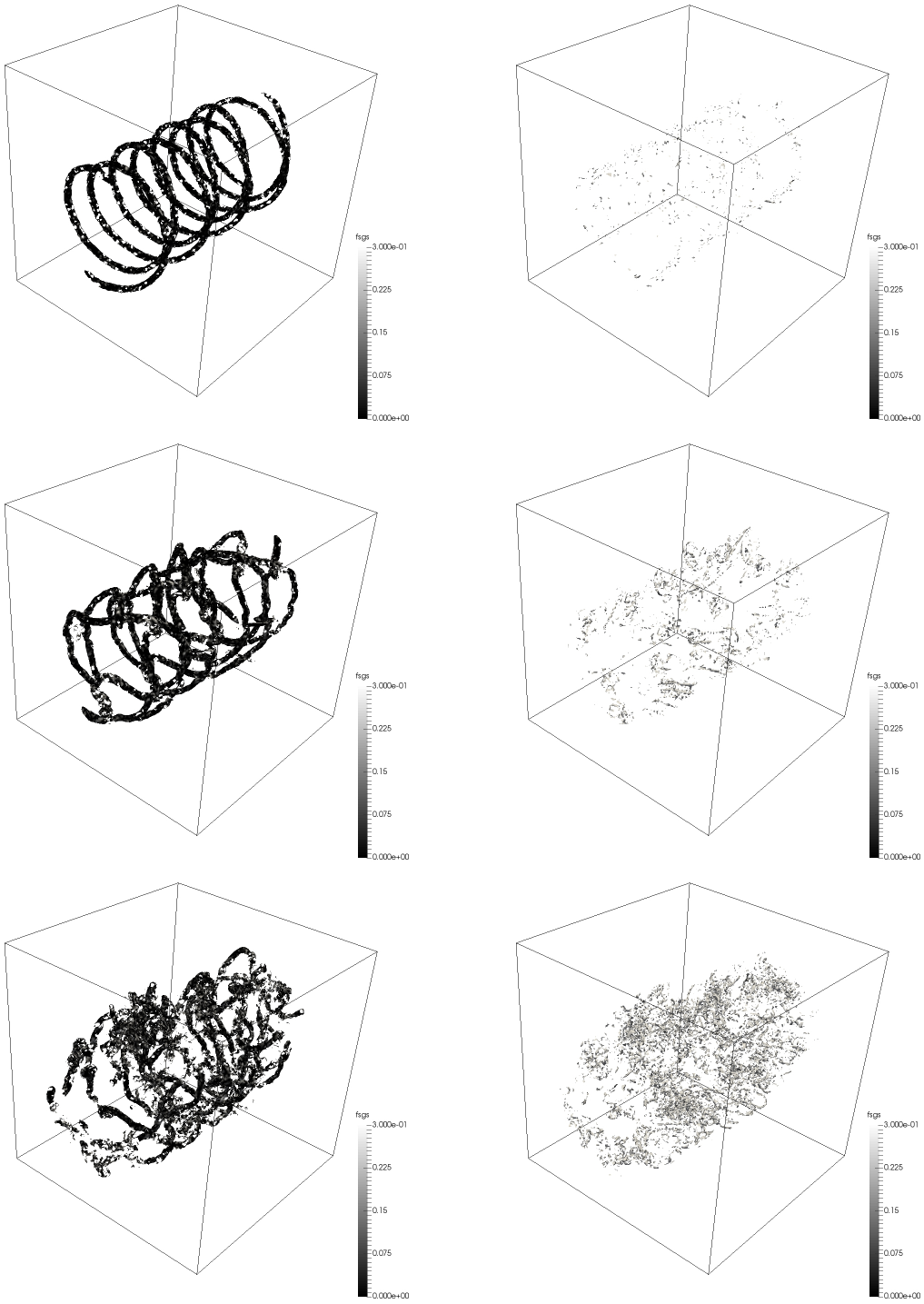

Figure 9. Iso-surfaces of vorticity colored by the sensor function at three different times $t = 2, 4, 6$ (resp. first, second and third rows) for the LES of the double helix configuration. Left column: iso-surfaces corresponding to values of sensor function between 0 and 0.3. Right column: iso-surfaces corresponding to values between 0.3 and 1.

Downloaded by PURDUE UNIVERSITY on February 2, 2019 | http://arc.aiaa.org | DOI: 10.2514/6.2017-4168

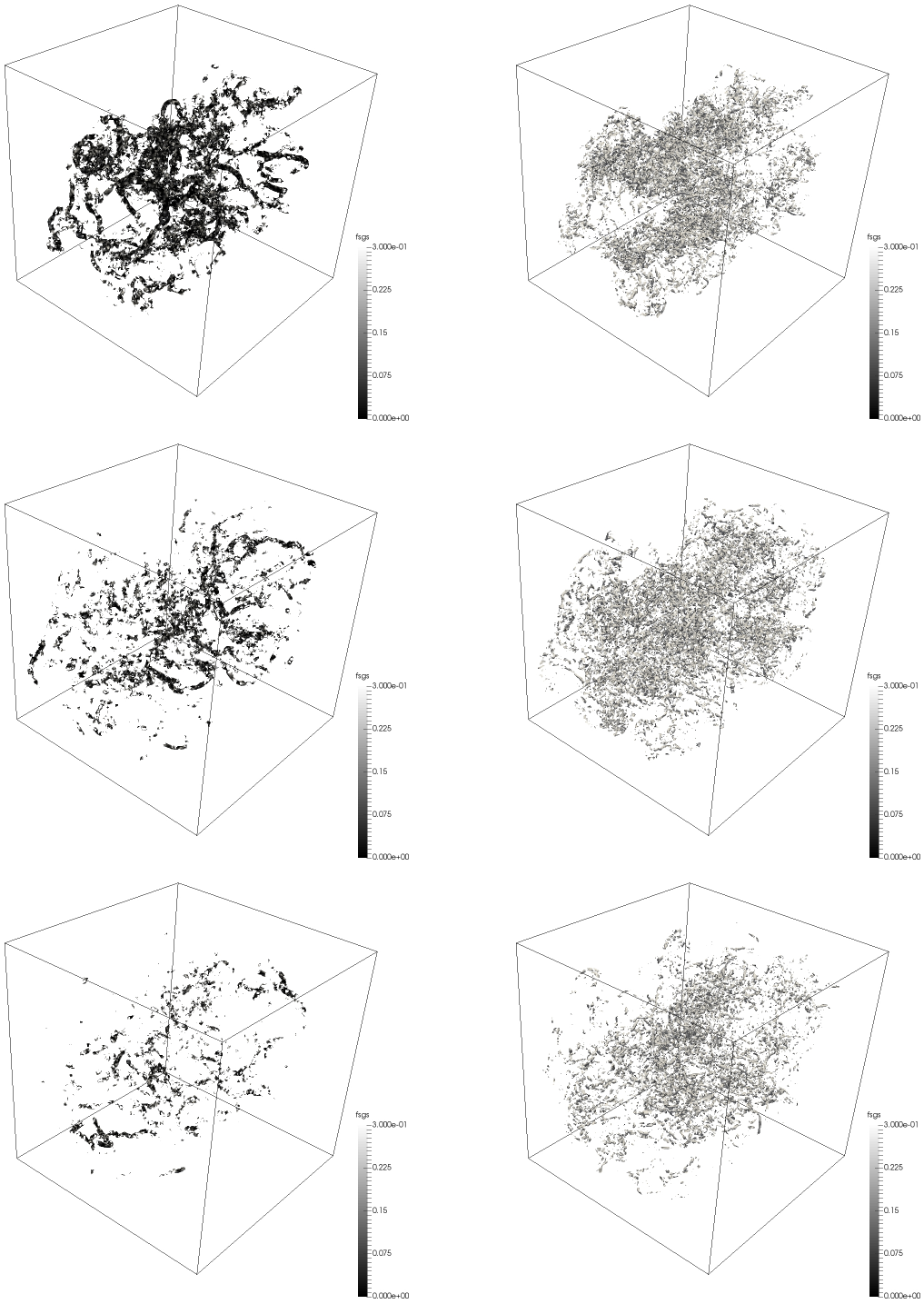

Figure 10. Iso-surfaces of vorticity colored by the sensor function at three different times $t = 2, 4, 6$ (resp. first, second and third rows) for the LES of the double helix configuration. Left column: iso-surfaces corresponding to values of sensor function between 0.3 and 1. Right column: iso-surfaces corresponding to values between 0.3 and 1.

Downloaded by PURDUE UNIVERSITY on February 2, 2019 | http://arc.aiaa.org | DOI: 10.2514/6.2017-4168

VI. Conclusion

In this paper, a novel SGS modeling concept based on a turbulence sensor has been developed. The turbulence sensor is built from the ratio of test and grid filtered enstrophy in order to determine the onset of transition or broadband turbulence locally in the flow. A damping function depending on the sensor is then defined and allows for a reduction of the modeled subgrid dissipation in such regions.

The present methodology has been assessed from LES computations of the Taylor-Green vortex flow at $Re = 5000$. It is found that the damping function successfully reduces the SGS dissipation at the early, transitional stages of the flow and progressively leads to a full activation of the subgrid model when turbulence is building up. The corresponding evolution of kinetic energy and dissipation is very well predicted and matches closely filtered DNS results, especially considering the coarse discretization of the LES study. The damping function has been coupled to several dissipative LES models and is found to improve all of them, underlying the flexibility of the method which can be used in conjunction with any existing SGS model. It must be emphasized that this approach is relatively simple, inexpensive and only the implementation of a test filter is required.

Finally, the model has been assessed for a newly developed numerical test case allowing for the fundamental study of rotor wake vortices. A coarse LES of this configuration with a pitch to vortex radius ratio $h/R = 1.1$, which is unstable due to the mutual inductance phenomenon, has been performed using the CvP model. Vizualisations of iso-surface of vorticity colored by the sensor function values have shown that the turbulence sensor is able to sort the coherent motion from the small-scale turbulence. However, locally high-values of the sensor function have been observed in the contour of coherent vortices. An improvement of the sensor behavior could be therefore obtained by smoothing the function which is a current topic of investigation.

Future work will aim at assessing the behavior of the present approach for wall-bounded turbulence and more complicated flow configurations, as well as its implementation in more practical flow solvers. Current work is also focused on determining accurately and locally the coherent scale using a variant of the CvP methodology.

Acknowledgments

The authors acknowledge financial support of the subcontract KSC-17-001 between Purdue University and Kord Technologies, Inc (Huntsville), conducting research under the US Navy Contract N68335-17-C-0159 STTR-Phase II, Purdue Proposal No. 00065007, Topic N15A-T002 entitled *Vortex Preserving and Consistent Large Eddy Simulations for Naval Applications*. The computing resources were provided by the Rosen Center for Advanced Computing (RCAC) at Purdue University and Information Technology at Purdue (ITaP).

References

[1]Smagorinsky, J., "General circulation experiments with the primitive equations," *Mon. Weather Rev.*, Vol. 91, No. 3, 1963, pp. 99–164.

[2]Kraichnan, R., "Eddy viscosity in two and three dimensions," *J. Atmo. Sci.*, Vol. 33, No. 8, 1976, pp. 1521–1536.

[3]Sagaut, P., *Large-Eddy simulation for incompressible flows: an introduction*, Springer Verlag, 2006.

[4]Germano, M., Piomelli, U., Moin, P., and Cabot, W., "A dynamic subgrid-scale eddy viscosity model," *Phys. Fluids*, Vol. 3, No. 7, 1991, pp. 1760–1765.

[5]Ghosal, S., Lund, T. S., Moin, P., and Akselvoll, K., "A dynamic localization model for Large-Eddy simulation of turbulent flows," *J. Fluid Mech.*, Vol. 286, 1995, pp. 229–255.

[6]Meneveau, C., Lund, T. S., and Cabot, W. H., "A Lagrangian dynamic subgrid-scale model of turbulence," *J. Fluid Mech.*, Vol. 319, 1996, pp. 353–385.

[7]Lamballais, E., Métais, O., and Lesieur, M., "Spectral-dynamic model for Large-Eddy simulations of turbulent rotating channel flow," *Theo. Comput. Fluid Dyn.*, Vol. 12, No. 3, 1998, pp. 149–177.

[8]Park, N., Lee, S., Lee, J., and Choi, H., "A dynamic subgrid-scale eddy viscosity model with a global model coefficient," *Phys. Fluids*, Vol. 18, No. 12, 2006, pp. 125109.

[9]Stolz, S., Schlatter, P., and Kleiser, L., "High-pass filtered eddy-viscosity models for Large-Eddy simulations of transitional and turbulent flow," *Phys. Fluids*, Vol. 17, 2005, pp. 065103.

[10]Hughes, T., Mazzei, L., and Jansen, K., "Large-Eddy Simulation and the variational multiscale method," *Computing and Visualization in Science*, Vol. 3, No. 1, 2000, pp. 47–59.

[11]David, E., *Modélisation des écoulements compressibles et hypersoniques: une approche instationnaire*, Ph.D. thesis, 1993.

[12]Ackermann, C. and Métais, O., "A modified selective structure function subgrid-scale model," *Journal of Turbulence*, Vol. 2, No. 1, 2001.

[13]Chapelier, J.-B. and Lodato, G., "A spectral-element dynamic model for the Large-Eddy simulation of turbulent flows," *J. Comput. Phys.*, Vol. 321, 2016, pp. 279–302.

[14]Farge, M., Schneider, K., and Kevlahan, N., "Non-Gaussianity and coherent vortex simulation for two-dimensional turbulence using an adaptive orthogonal wavelet basis," *Phys. Fluids*, Vol. 11, 1999, pp. 2187.

[15]Farge, M. and Schneider, K., "Coherent vortex simulation (CVS), a semi-deterministic turbulence model using wavelets," *Flow Turb. Comb.*, Vol. 66, No. 4, 2001, pp. 393–426.

[16]Schneider, K., Farge, M., Pellegrino, G., and Rogers, M. M., "Coherent vortex simulation of three-dimensional turbulent mixing layers using orthogonal wavelets," *J. Fluid Mech.*, Vol. 534, 2005, pp. 39–66.

[17]Farge, M., Pellegrino, G., and Schneider, K., "Coherent vortex extraction in 3D turbulent flows using orthogonal wavelets," *Phys. Rev. Letters*, Vol. 87, No. 5, 2001, pp. 054501.

[18]Karamanos, G. and Karniadakis, G., "A spectral vanishing viscosity method for Large-Eddy simulations," *J. Comput. Phys.*, Vol. 163, No. 1, 2000, pp. 22–50.

[19]Pasquetti, R., "Spectral vanishing viscosity method for Large-Eddy simulation of turbulent flows," *J. Sci. Comput.*, Vol. 27, No. 1-3, 2006, pp. 365–375.

[20]Bogey, C. and Bailly, C., "Large-Eddy simulations of transitional round jets: influence of the Reynolds number on flow development and energy dissipation," *Phys. Fluids*, Vol. 18, No. 6, 2006, pp. 065101.

[21]Bogey, C. and Bailly, C., "Computation of a high Reynolds number jet and its radiated noise using Large- Eddy simulation based on explicit filtering," *Comput. Fluids*, Vol. 35, No. 10, 2006, pp. 1344–1358.

[22]Grinstein, F. F., Margolin, L. G., and Rider, W. J., *Implicit Large-Eddy Simulation: computing turbulent fluid dynamics*, Cambridge university press, 2007.

[23]Hickel, S., Adams, N. A., and Domaradzki, J. A., "An adaptive local deconvolution method for implicit LES," *J. Comput. Phys.*, Vol. 213, No. 1, 2006, pp. 413–436.

[24]Hickel, S. and Adams, N., "On implicit subgrid-scale modeling in wall-bounded flows," *Phys. Fluids*, Vol. 19, No. 10, 2007, pp. 105106.

[25]Garnier, E., Mossi, M., Sagaut, P., Comte, P., and Deville, M., "On the use of shock-capturing schemes for large-eddy simulation," *J. Comput. Phys.*, Vol. 153, No. 2, 1999, pp. 273–311.

[26]Mittal, R. and Moin, P., "Suitability of upwind-biased finite difference schemes for large-eddy simulation of turbulent flows," *AIAA Journal*, Vol. 35, No. 8, 1997, pp. 1415–1417.

[27]Nagarajan, S., Lele, S., and Ferziger, J., "A robust high-order compact method for large eddy simulation," *J. Comput. Phys.*, Vol. 191, 2003, pp. 392–419.

[28]Leonard, A., "Energy cascade in large-eddy simulations of turbulent fluid flows," *Adv. Geophys.*, Vol. 18, 1974, pp. 237–248.

[29]Lesieur, M. and Comte, P., "Favre filtering and macro-temperature in Large-Eddy simulations of compressible turbulence," *CR. Acad. Sci. Serie II*, Vol. 329, No. 5, 2001, pp. 363–368.

[30]Lesieur, M., Métais, O., and Comte, P., *Large-Eddy simulations of turbulence*, Cambridge University Press, 2005.

[31]Lesieur, M. and Metais, O., "New trends in Large-Eddy simulations of turbulence," *Ann. Rev. Fluid Mech.*, Vol. 28, No. 1, 1996, pp. 45–82.

[32]Erlebacher, G., Hussaini, M., Speziale, C., and Zang, T., "Toward the Large-Eddy simulation of compressible turbulent flows," *J. Fluid Mech.*, Vol. 238, No. 1, 1992, pp. 155–185.

[33]Lele, S., "Compact finite difference schemes with spectral-like resolution," *J. Comput. Phys.*, Vol. 103, No. 1, 1992, pp. 16–42.

[34]Metais, O. and Lesieur, M., "Spectral Large-Eddy Simulation of isotropic and stably stratified turbulence," *J. Fluid Mech.*, Vol. 239, No. 1, 1992, pp. 157–194.

[35]Vreman, A., "An eddy-viscosity subgrid-scale model for turbulent shear flow: Algebraic theory and applications," *Phys. Fluids*, Vol. 16, No. 10, 2004, pp. 3670–3681.

[36]Spyropoulos, E. T. and Blaisdell, G. A., "Evaluation of the dynamic model for simulations of compressible decaying isotropic turbulence," *AIAA J.*, Vol. 34, No. 5, 1996, pp. 990–998.

[37]Lilly, D. K., "A proposed modification of the Germano subgrid-scale closure method," *Physics of Fluids A: Fluid Dynamics (1989-1993)*, Vol. 4, No. 3, 1992, pp. 633–635.

[38]Bagai, A. and Leishman, J. G., "Flow visualization of compressible vortex structures using density gradient techniques," *Exp. Fluids*, Vol. 15, No. 6, 1993, pp. 431–442.

[39]Nemes, A., Jacono, D. L., Blackburn, H. M., and Sheridan, J., "Mutual inductance of two helical vortices," *J. Fluid Mech.*, Vol. 774, 2015, pp. 298–310.

Downloaded by PURDUE UNIVERSITY on February 2, 2019 | http://arc.aiaa.org | DOI: 10.2514/6.2017-4168